Article:
Gibson, F.G., Paggiosi, M.A., Handforth, C. et al. (2025) Altered vertebral biomechanical properties in prostate cancer patients following androgen deprivation therapy. Bone, 195. 117465. ISSN: 8756-3282

https://doi.org/10.1016/j.bone.2025.117465

Bone 195 (2025) 117465

Contents lists available at ScienceDirect

Bone

journal homepage: www.elsevier.com/locate/bone

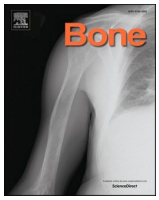

Full Length Article

Altered vertebral biomechanical properties in prostate cancer patients following androgen deprivation therapy

Fiona G. Gibson [a,b], Margaret A. Paggiosi [c], Catherine Handforth [c], Janet E. Brown [c], Xinshan Li [a,b], Enrico Dall'Ara [b,c], Stefaan W. Verbruggen [a,b,d,*]

[a] School of Mechanical, Aerospace and Civil Engineering, The University of Sheffield, Sheffield, United Kingdom
[b] INSIGNEO Institute for in silico Medicine, The University of Sheffield, Sheffield, United Kingdom
[c] Division of Clinical Medicine, School of Medicine & Population Health, The University of Sheffield, Sheffield, United Kingdom
[d] Centre for Bioengineering, School of Engineering and Materials Science, Queen Mary University of London, London, United Kingdom

ARTICLE INFO

Keywords:
Prostate cancer
Androgen deprivation therapy (ADT)
Vertebral biomechanics

ABSTRACT

Androgen deprivation therapy (ADT) for localised and metastatic prostate cancer (PCa) is known to improve survival in patients but has been associated with negative long-term impacts on the skeleton, including decreased bone mineral density (BMD) and increased fracture risk. Generally, dual-enery X-ray absorptiometry (DXA) measurements of areal BMD (aBMD) of vertebrae are used clinically to assess bone health. However, a prediction of vertebral bone strength requires information that aBMD cannot provide, such as geometry and volumetric BMD (vBMD). This study aims to investigate the effect of ADT on the densitometric (aBMD, trabecular vBMD, integral vBMD) and mechanical integrity (failure load and failure strength) of vertebrae, using a combination of DXA, quantitative computed tomography (QCT) and finite element (FE) modelling. For the FE analyses, 3D models were reconstructed from QCT images of 26 ADT treated patients, and their matched controls, collected as part of the ANTELOPE clinical trial. The ADT treated group experienced significantly decreased trabecular and integral vBMD (trabecular vBMD: −18 %, $p < 0.001$, integral vBMD: −11 %, $p < 0.001$) compared to control patients that showed no significant temporal changes (trabecular vBMD $p = 0.037$, integral vBMD $p = 0.56$). A similar trend was seen in the ADT treated group for the failure load and failure strength, where a decrease of 14 % was observed ($p < 0.001$). When comparing the proficiency in predicting the mechanical properties from densitometric properties, the integral vBMD performed best in the pooled data ($r = 0.86$–0.87, $p < 0.001$) closely followed by trabecular vBMD ($r = 0.73$–0.75, $p < 0.001$) with aBMD having a much weaker predictive ability ($r = 0.19$–0.21, $p < 0.01$). In conclusion, ADT significantly reduced both the densitometric properties and the mechanical strength of vertebrae. A stronger relationship between both trabecular vBMD and integral vBMD with the mechanical properties than the aBMD was observed, suggesting that such clinical measurements could improve predictions of fracture risk in prostate cancer patients treated with ADT.

1. Introduction

Prostate cancer (PCa) is the most common non-skin cancer among men [1] and the median age at PCa diagnosis is around 66 years [2]. The effects of the disease itself, its treatment and the age of many PCa patients cumulatively give rise to substantial skeletal morbidity [3,4]. Androgen deprivation therapy (ADT), which reduces the growth and development of androgen-dependent PCa cells, by reducing testosterone levels, is a standard of care for many men diagnosed with PCa. Numerous studies have demonstrated the benefits of ADT in improving survival in patients, with both localised and metastatic PCa [5,6]. However, since bone health is also dependent upon androgens, ADT is associated with negative impacts on the skeleton, including a decrease in bone mineral density (BMD) [7] and an increase in fracture risk [8–10].

Studies have shown that ADT disrupts the bone remodelling cycle. Testosterone and oestradiol levels, important factors in the maintenance of adult bone, are reduced following ADT [11,12]. Greenspan et al. described how a reduction in testosterone was significantly correlated with a reduction in areal BMD (aBMD) after 6–12 months of ADT [13]. Other studies have shown a significant decrease in total hip, femoral

* Corresponding author at: Centre for Bioengineering, School of Engineering and Materials Science, Queen Mary University of London, London, United Kingdom.
E-mail address: s.verbruggen@qmul.ac.uk (S.W. Verbruggen).

https://doi.org/10.1016/j.bone.2025.117465
Received 10 July 2024; Received in revised form 26 February 2025; Accepted 18 March 2025
Available online 19 March 2025

neck, and lumbar spine areal BMD (aBMD) by 1.5–4.0 % annually following commencement of ADT, which exceeds both normal annual bone loss for healthy ageing males and that of postmenopausal women (2.5 %) [14,15]. Despite this, prospective studies reporting bone loss with ADT in men with nonmetastatic PCa have often not evaluated the association of fractures with ADT. However, the correlation of fractures with ADT in PCa patients was evaluated by three large retrospective studies that reported these patients having a 21–37 % higher risk of fracture compared to PCa patients who were not treated with ADT [8,16,17]. Smith and colleagues also reported that vertebral fractures were 18 % more likely to occur following ADT, as well as an overall fracture risk increase of 13 % [16].

Dual energy X-ray absorptiometry (DXA) is the 'gold standard' clinical method for measuring areal BMD (aBMD, in g/cm^2) and determining fracture risk, as part of a standard comprehensive fracture risk assessment. However, fracture risk is also associated with bone strength, which in turn is dependent on bone quantity and quality. As a 2D projected measurement, DXA cannot provide information on the 3D shape and the large regional variation in vertebral geometries, and the distribution of BMD, throughout the bone volume. Moreover, DXA measurements of aBMD in the vertebral body are affected by either the presence of the posterior elements (anterior-posterior DXA) or by the ribs or pelvis (lateral DXA). Therefore, to fully capture bone strength, a three-dimensional (3D) quantitative evaluation of the bone biomechanics is necessary. Quantitative computed tomography (QCT) has been used to quantify volumetric BMD (vBMD, in g/cm^3) at various sites such as the spine, hip and femur [18], as a measure that more accurately captures the 3D distribution of mineral in bone tissue. QCT has several advantages over DXA as it can perform sub-regional analysis whilst incorporating the 3D geometry of bone [18].

This more holistic approach has recently been employed in a longitudinal, observational clinical trial of PCa patients commencing ADT (the ANTELOPE trial) [19]. In this study, 31 men with non-metastatic PCa, scheduled to commence ADT, were recruited from urology/oncology clinics at the Royal Hallamshire Hospital, Sheffield, along with recruitment of 30 healthy male volunteers matched by age (± 5 years), height (± 5 cm) and body mass index (BMI) (± 5 kg/m^2) to the patients in the ADT treatment group. This patient and volunteer number was chosen to reflect the need for powering the ANTELOPE primary endpoint, which was a change in 12-month vBMD at the distal radius. A range of assessments including aBMD at hip and lumbar spine by DXA scan, vBMD and other microarchitectural parameters at the non-dominant radius by high-resolution peripheral quantitative computed tomography (HR-pQCT), bone turnover markers and other measurements of muscle function and strength and body composition were carried out at baseline and again at 12 months. Overall, the ADT treated group experienced a significant decrease in lumbar spine aBMD ($p < 0.001$), radius trabecular vBMD ($p < 0.001$) and cortical vBMD ($p < 0.001$), and ultimate failure load at the radius ($p = 0.03$). Full details of trial design and inclusion/exclusion criteria have been published [19].

Nevertheless, little is known about the effect of ADT on the vertebral strength. QCT images can be used to create 3D biomechanical models, using finite element (FE) analysis of the vertebra to estimate the bone strength [52]. Subject specific FE models have been used extensively to study the biomechanical response of bones to loading [20,21]. This technique is being used increasingly in bones affected by diseases such as osteoporosis [22] and different types of cancer including breast, colorectal and renal cell carcinoma [23]. It has also been used to study the effect of treatments and has been proven to predict vertebral strength more accurately than DXA in individuals without skeletal diseases [24,25] and with osteoporosis [26].

Despite studies investigating the effect of ADT on the peripheral strength of the distal radius using HR-pQCT [27], and femoral strength and fracture risk have been estimated using biomechanical computed tomography (BCT) [28], the vertebral strength is yet to be assessed using FE models based on QCT images of the vertebra. Therefore, the overall aim of this study (pre-planned in the ANTELOPE design), was to uniquely include a comparison of the effect of ADT on the aBMD, measured in the ANTELOPE design, with QCT based vBMD and FE estimated mechanical strength of vertebrae.

2. Materials and methods

2.1. Study design and participants

The overall study design of the ANTELOPE trial and demographics of the participants have been described elsewhere in Handforth et al. (2024) [19]. Ethical approval was obtained from the South Yorkshire Research Ethics Committee in October 2016 (IRAS ID 206171). Out of the 31 patients in Group A (ADT treated) of the ANTELOPE trial, 29 patients completed all study assessments and 26 had a matched control making up the cohort within this study. All patients were received intravenous ADT and there was no presence of vertebral fracture in any of the patients T12 vertebra assessed in this study.

2.2. DXA and aBMD measurements

All study participants underwent a posterior-anterior DXA (Discovery A, Hologic, USA) of the lumbar spine, at baseline and 12 months, at the NIHR Clinical Research Facility, Northern General Hospital, Sheffield. Lumbar spine (L1-L4) aBMD (g/cm^2) was also measured.

2.3. QCT and vBMD measurements

The first cohort from 2017 was scanned using the GE LightSpeed VCT (GE Healthcare, Milwaukee, WI) in the radiology department at the Northern General Hospital, Sheffield, whilst the follow-up scans in 2018 along with all second cohort scans were scanned using the Toshiba Aquilion ONE (Toshiba Medical Systems, Tokyo, Japan) at the same hospital. Quality assurance was performed once per month using a Mindways phantom (Mindways Software, Inc., Austin, TX, USA) on both scanners. All scans were performed in the anteroposterior position, using the same noise index. The QCT protocol included a single scan from the superior edge of the T12 vertebra to the T12/L1 margin. For the GE scanner, the tube voltage was 120 kV and the mean tube current was set at 360 mA and were reconstructed with a voxel size of 0.937 × 0.937 × 0.625 mm. For the Toshiba scanner, the tube voltage was also 120 kV, the mean tube current was set at 250 mA and a voxel size of 0.976 × 0.976 × 0.5 mm.

Each QCT scan, for both the GE LightSpeed VCT and the Toshiba Aquilion ONE, contained a solid inline calibration phantom (Image Analysis, Inc., Columbia, KY, USA), with rods of 0, 75, and 150 mg/cm^3 equivalent BMD. The densitometric calibration was computed for each individual scan using a standard approach, which assumes a linear relationship between the average Hounsfield units (HU) and the known mean values of equivalent BMD of each rod. To do so, one region of interest (ROI) was defined manually within each insertion of the phantom (ImageJ 1.54i, [29,30]. The ROIs were defined as square regions centred within each calibration rod with length equal to half the edge length of the rod (12.5 mm). Mean HU values over the same 10 slices were used to perform the linear regression analysis with the known values of equivalent BMD for all three rods for calibration. The individually and independently calibrated QCT scans removes any differences in scanning protocol, the type of scanner, and the effect of these on the current study.

For the assessment of trabecular vBMD, from each QCT an ellipse shaped ROI was identified (ImageJ) in the anterior most region of the vertebral body, in the trabecular portion only. The ellipse was identified by creating a circular region of interest in the vertebral body, ensuring the cortical portion was included. The height and the width of the circular region were then reduced by 60 % and 20 %, respectively. After that, the ellipse was moved to ensure it was in the top half of the

vertebral body and 10 % away (in terms of width) from all edges. This ROI was extended to include the 10 central slices of the vertebral body. HU values within the ROI for all slices were converted into vBMD using the densitometric calibration identified as described above. For the integral vBMD, the FE software Ansys Workbench (2021R1) was used to select a ROI for all the elements in each vertebral body, excluding the posterior elements and processes, incorporating both the cortical and trabecular regions. The integral vBMD (g/cm^3) was then calculated as the sum of the individual element's bone mineral content (element BMD multiplied by element volume) divided by the total volume of the vertebral body ROI.

2.4. FE models and mechanical properties

During the FE analysis, one patient from the ADT group was removed along with the matched control due to difficulty separating the intended T12 vertebra from the vertebra above (T11) in the segmentation stage.

3D models of each vertebra were reconstructed from the QCT images using 3D-Slicer (3D-slicer 4.1120210226, [https://www.slicer.org/] [31]). Ansys SpaceClaim (Ansys® 2021R1, ANSYS, Inc) was then used to prepare the models to ensure accurate meshing by removing anomalous sharp edges and floating elements. The models were then imported into Ansys Mechanical (Ansys® 2021R1, ANSYS, Inc) and meshed using quadratic (10 nodes) tetrahedral elements with maximal edge length of 1 mm [23], following a mesh convergence analysis.

Bone was modelled as a heterogenous, isotropic, and elastic-plastic material [23]. Bonemat (BONEMAT® 3.2, 2013) was used to assign the heterogeneous, linear material properties for each vertebra model based on the patient-specific densitometry calibration described above and phenomenological relationships [Eqs. (1) and (2)] [32,33] (Fig. 1A).

$$\rho_{QCT} = \rho_{app} \times 0.6 \ [g/cm^3] \quad (1)$$

$$E = 4730\rho_{app}^{1.56} \ [MPa] \quad (2)$$

The plastic behaviour of bone was modelled in Ansys Workbench using an isotropic Von Mises yield criterion, based on a density-strength relationship [Eq. (3)] [34], and a 95 % reduction in the post-yield elastic modulus [Eq. (4)] [33,35].

$$\sigma_{y1} = 21.7\rho_{app}^{1.52} \ [MPa] \quad (3)$$

$$E_{py} = 0.05 \times E \ [MPa] \quad (4)$$

Each vertebra model was aligned to ensure the loading was applied perpendicular to the endplates of the vertebral body by creating best-fit planes on the superior and inferior endplates and aligning the vertebra to the average of these two planes in Ansys SpaceClaim. The superior and inferior surfaces of the endplates were also identified and labelled manually using anatomical landmarks on the vertebral body, to create a surface (in SpaceClaim) for ease of applying the boundary conditions (Fig. 2). The models were loaded in uniaxial compression on the superior endplate with a displacement of 1.9 % of the minimum vertebral height (h), calculated as the minimum distance between the superior and inferior surfaces of the vertebral body. An apparent deformation of 1.9 % has been experimentally proven to produce ultimate stress in vertebral bodies [25,36]. The elements on the inferior endplate were fixed in all directions.

Load-displacement curves (Fig. 1B), which were created from the reaction force (sum of the reaction forces on the inferior endplate) and the imposed displacement, were used to calculate the structural properties. Specifically, stiffness was defined as the slope of the linear portion of the curve and the failure load as the maximum force of the nonlinear portion (load at 1.9 % of apparent deformation) (Fig. 1B&C). Material properties were computed by normalising the structural properties with the sample dimensions. In particular, normalised stiffness was defined by dividing the stiffness by the ratio CSA/h, where cross sectional area (CSA) was calculated as the average CSA of the vertebral body and vertebral height (h) was calculated as the minimum distance between the inferior and superior endplates, and the failure strength as the failure load divided by CSA.

2.5. Statistical analysis

A Wilcoxon paired test was used to compare the densitometric and FE predicted mechanical properties between baseline and 12 months for both groups (significance was considered at $p < 0.05$, *p < 0.05, **$p <$ 0.01, ***$p < 0.0001$). A Wilcoxon unpaired test (Mann-Whitney U test) was used to test whether the percentage differences between baseline and 12 months within the treated group was significantly different from the control group. A Wilcoxon paired one tail test was used to evaluate if there was a significantly positive or negative trend in the densitometric, and FE predicted mechanical properties between baseline and 12 months.

Linear regressions were calculated between the percentage difference between the two time points for the FE failure load, failure strength and densitometric variables for the pooled and treated and control groups. The Pearson's correlation coefficients with corresponding p-values of the predictions were calculated for all linear regressions. Where an $r \leq 0.3$ represents a weak correlation, $0.3 < r < 0.7$ is

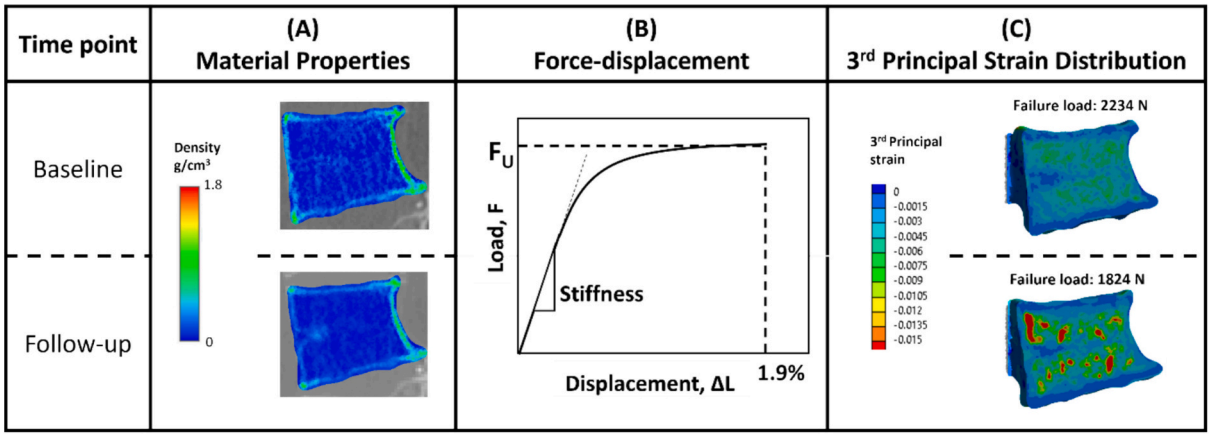

Fig. 1. Illustration of the outputs from the FE analysis at both time points. (A) Distribution of the BMD within the vertebral body taken from Bonemat, where blue is low BMD and yellow/red is high BMD. (B) Load-displacement curve used to calculate the stiffness and failure load from the FE results. (C) An example of the 3rd principal strain distribution within a model with the associated failure load. (For interpretation of the references to colour in this figure legend, the reader is referred to the web version of this article.)

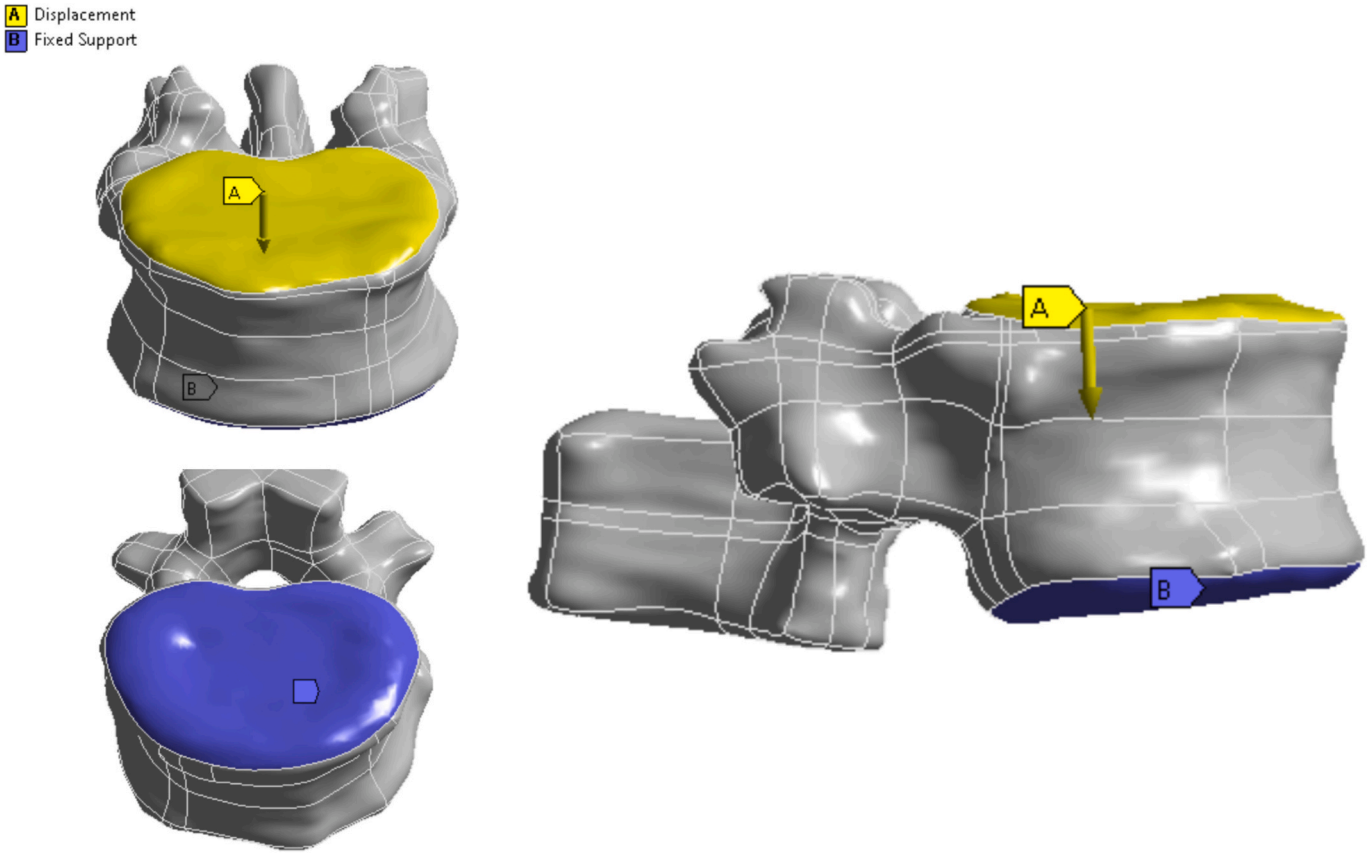

Fig. 2. Application of boundary conditions illustrated using a T12 vertebra of a 79-year-old patient. (A) The displacement applied to the superior endplate. (B) The fixed support applied to the inferior endplate.

moderate correlation and $0.7 < r \leq 1$ is a strong correlation, with p-values where significance was considered for $p < 0.05$ and the significance levels were described by *p < 0.05, **$p < 0.01$, ***$p < 0.001$.

3. Results

Table 1 shows the patient demographics for the treated group and matched control detailing the age, height and BMI for each patient as well as the average and standard deviation showing no significant

Table 1
Patient demographics data for the treated and control groups (25 subjects per group) used in this study including age, height, and BMI.

Treated	Age (years)	Height (cm)	BMI (kg/m^2)	Matched Control	Age (years)	Height (cm)	BMI (kg/m^2)
A01	72	178.8	29.0	C01	74	192.3	31.4
A02	80	173.9	26.7	C15	80	175.2	26.3
A03	67	165.9	21.9	C32	64	171.7	23.5
A05	67	179.2	27.3	C25	71	182.0	24.9
A06	70	180.6	31.0	C06	68	182.8	27.1
A07	72	173.2	23.1	C26	71	173.0	20.4
A10	71	191.1	32.7	C09	63	188.1	29.6
A13	65	169.7	27.3	C16	82	169.0	29.7
A16	82	169.8	32.7	C11	79	175.0	30.7
A17	76	181.0	24.1	C20	73	178.0	24.2
A19	79	180.3	24.1	C30	75	181.0	25.5
A20	74	181.7	28.6	C03	77	180.1	30.1
A21	71	167.7	25.8	C14	74	168.2	26.8
A23	64	172.4	25.9	C08	53	184.4	26.9
A24	78	174.2	25.8	C02	76	169.0	22.3
A25	73	170.8	28.3	C04	73	173.3	26.2
A27	80	167.6	25.8	C05	78	170.4	26.9
A28	76	175.4	27.8	C12	78	179.0	32.1
A30	76	176.9	30.1	C19	75	180.8	34.9
A32	80	160.7	26.9	C21	78	159.8	22.7
A33	76	163.4	34.4	C23	77	163.2	31.8
A34	72	175.4	31.3	C31	71	171.0	27.6
A35	73	182.2	24.3	C24	73	184.5	23.9
A37	80	171.3	23.9	C17	78	169.0	24.9
A38	67	165.4	23.9	C10	70	161.0	29.3
Average (±SD)	74 ± 5	174.3 ± 6.8	27.4 ± 3.3	Average (±SD)	73 ± 6	175.9 ± 8.0	27.1 ± 3.5

differences between the groups. ADT reduced both densitometric and mechanical properties in men with PCa (Table 2). On average, between the baseline and 12-month visits, the patients receiving ADT displayed a significant reduction in aBMD (aBMD: −4 %, $p < 0.01$), whilst the aBMD in the control group increased (+2.3 %, $p < 0.05$). Trabecular vBMD at 12 months had a larger decrease than aBMD for the patients who received ADT (trabecular vBMD: −18 %, $p < 0.01$), whilst the control group showed no significant change ($p = 0.056$). Integral vBMD also had a larger decrease than aBMD for patients receiving ADT (integral vBMD: −11 %, $p < 0.01$), whilst the control group showed no significant change at 12 months ($p = 0.75$). The FE analysis predicted an even larger decrease in mechanical properties for the patients receiving ADT than both aBMD and integral vBMD but similar to trabecular vBMD (stiffness: −14 %, $p < 0.01$; failure load: −16 %, $p < 0.01$; normalised stiffness: −14 %, $p < 0.01$; failure strength: −16 %, $p < 0.01$), compared to the control group. The change between baseline and 12 months in the treated group with respect to the change in the matched control was also significant for all densitometric and mechanical properties (Table 2, $p < 0.05$).

Fig. 3 shows a representative model from the FE analysis of a subject in the treated group (A19), where the mechanical properties have decreased by 17–20 % over 12 months. The resulting decrease in mechanical properties has driven an increase in compressive strain within the vertebral body. This is highlighted by the increase in red regions within the vertebral body at follow-up (Fig. 3A) as well as an increase in frequency of higher strains at follow-up shown in the histogram (Fig. 3B). The shear strain distributions in Fig. 4A show the higher shear strain in the 12-month vertebra compared to the baseline for the same patient. The shear strains observed at follow-up are around 10 % smaller than the compressive strains, implying compression is the main failure mode. Fig. 4B highlights the higher plastic strains in similar regions to the high compressive strains, suggesting there is a higher risk of fracture in these regions.

Fig. 5 details the aBMD, vBMD, integral vBMD and failure strength for all patients in the control and treated group at baseline and 12 months. The violin plots of the aBMD show a similar distribution in both the control and treated groups, with the line plots confirming the changes in both groups between baseline and 12 months, where the blue (control) lines had a tendency towards positive gradient (aBMD: $p < 0.001$), whereas the red (treated) lines trended towards a negative gradient (aBMD: $p < 0.001$). Whilst the trabecular vBMD, integral vBMD and failure strength had no trend in the control group, the negative trend in the treated group was significant (trabecular vBMD: $p < 0.001$, integral vBMD: $p < 0.001$, failure strength: $p < 0.001$). The vBMD, integral vBMD and failure strength all had a smaller range in the control group and the treated group.

The correlation between the densitometric parameters (aBMD, vBMD and integral vBMD) and the normalised mechanical properties was evaluated for the pooled data as well as the respective treated and control groups at both time points (Fig. 6). Trabecular vBMD and integral vBMD were both found to be a better predictor of bone strength than aBMD. A weak but significant correlation was found between the percentage change in aBMD and the percentage change in failure load and failure strength for the pooled data ($r = 0.28$–0.44, $p < 0.01$). Whereas the correlations between the pooled data for percentage change in trabecular vBMD or integral vBMD and the percentage change in failure load and failure strength were strong ($r = 0.78$–0.92, $p < 0.001$ for trabecular vBMD; $r = 0.88$–0.96, $p < 0.001$ for integral vBMD) (Fig. 6).

4. Discussion

This study is the first to evaluate the effect of ADT on the biomechanical properties of the vertebra in PCa patients. It demonstrates a more dramatic decrease in vertebral mechanical integrity than those predicted using standard DXA measurements of aBMD. By reconstructing QCT scans, FE models predicted a significant decrease in all densitometric and mechanical properties following 12 months of ADT. It was found that trabecular vBMD and integral vBMD measured *via* QCT correlated well with FE analyses outputs, indicating a significantly better prediction of mechanical properties at T12 than aBMD measured by DXA at L1-L4.

Previous studies have shown a decrease in aBMD of 1.5–4 % annually following commencement of ADT [14,15] and the ANTELOPE study also demonstrated a significant decrease in aBMD following ADT after 12 months, at 4 % [19]. Due to the high number of trabeculae within the vertebra, the highly vascular nature of trabecular bone, and the intravenous method used to administer ADT, the vertebra is at a higher risk of a reduction in BMD. In this study, similar but amplified trends were observed in the treated group for trabecular vBMD and integral vBMD, reducing by 17 % and 11 % respectively over 12 months. QCT scans have been adopted in previous studies to assess the trabecular vBMD and found similar trends after 1 year of ADT [37,38]. Similar amplified trends to this study were observed by Smith et al. [38] who reported a reduction of 3.3 % in lumbar aBMD and a reduction of 8.5 % in vBMD after 48 weeks of ADT. Sato et al. [37] reported also significant reduction in lumbar spine vBMD of 17.9 % following 12 months of ADT.

The ADT treated group experienced a notable decrease in mechanical properties, with a 14–16 % decrease in failure load, stiffness, failure strength, and normalised stiffness, compared to a 4 % decrease observed in aBMD. FE analyses has been shown to amplify the changes seen in

Table 2
Summarised data for densitometric (aBMD, trabecular vBMD, integral vBMD) and estimated mechanical properties (stiffness, failure load, normalised stiffness, and failure strength). Average and standard deviation are reported for each group and time point. Percentage differences (% diff) computed between the time points and *p*-values were reported (1). *P*-values were also reported to test the significance of the difference between the treated group and the matched control group (2).

	Control				Treated				p-Value[2]
	Baseline	12 Months	% diff	P-value[1]	Baseline	12 Months	% diff	P-value[1]	
aBMD (g/cm^2)	1.09 ± 0.18	1.12 ± 0.19	+2.3 %	0.0006	1.14 ± 0.17	1.09 ± 0.17	−4.0 %	0.0002	<0.0001
Trab vBMD (g/cm^3)	0.11 ± 0.036	0.11 ± 0.029	−4.9 %	0.037	0.13 ± 0.06	0.10 ± 0.05	−18 %	0.0004	0.011
Integral vBMD (g/cm^3)	0.21 ± 0.046	0.20 ± 0.035	+0.67 %	0.56	0.23 ± 0.06	0.20 ± 0.05	−11 %	0.0002	0.0002
Stiffness (kN/mm)	39.0 ± 16.3	37.7 ± 11.4	+6.9 %	0.73	45.1 ± 18.6	36.6 ± 13.8	−14 %	<0.0001	0.0004
Failure load (kN)	3.03 ± 1.27	2.94 ± 0.93	+2.4 %	0.69	3.45 ± 1.31	2.76 ± 0.91	−16 %	<0.0001	<0.0001
Normalised stiffness (MPa)	568 ± 218	559 ± 136	+7.8 %	0.97	754 ± 390	618 ± 314	−14 %	0.0003	0.0004
Failure strength (MPa)	1.79 ± 0.61	1.75 ± 0.40	+2.9 %	0.94	2.25 ± 1.10	1.81 ± 0.88	−16 %	0.0002	<0.0001

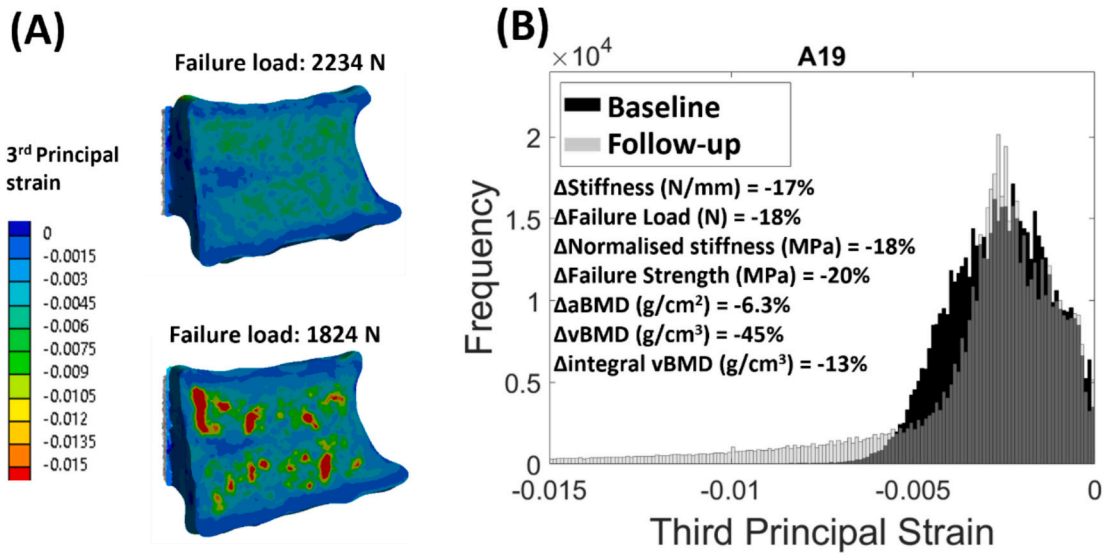

Fig. 3. Representative result from the FE analysis showing the local increases (red) in 3rd principal strain distribution (A) in the vertebral body and a histogram of the 3rd principal strain in the vertebral body where time point 2 has a higher proportion of strains in the higher strain region (B). (For interpretation of the references to colour in this figure legend, the reader is referred to the web version of this article.)

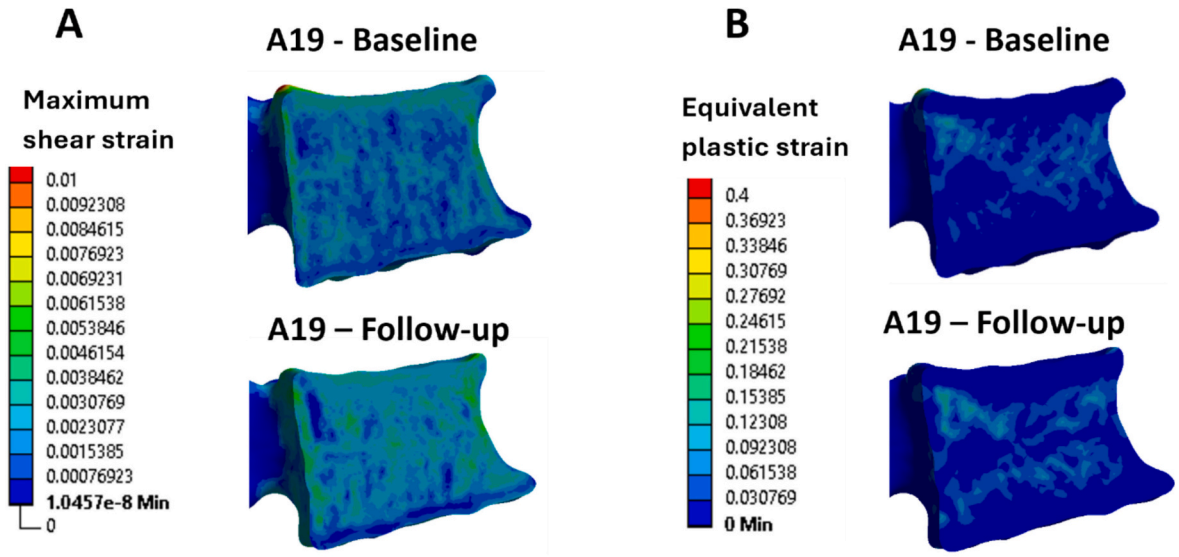

Fig. 4. Representative result from the FE analysis showing the local increases (red) in maximum shear strain distribution (A) and equivalent plastic strain (B) in the vertebral body. (For interpretation of the references to colour in this figure legend, the reader is referred to the web version of this article.)

aBMD from DXA in osteoporotic patients [39,40]. This could be explained by accounting for the 3D distribution of BMD, which has been shown to be indicative of strength gains [40], and cortical thickness, which has also proven to be important when predicting fracture risk [41]. In addition, FE models are a better predictor of bone strength (failure load) than estimations from aBMD [39] and trabecular vBMD [25], and are highly correlated with experimental results [42].

Areal BMD showed a low predictive ability for mechanical properties ($r = 0.28$–0.46), whereas vBMD and integral vBMD exhibited a strong correlation with mechanical properties ($r = 0.78$–0.92 for trabecular vBMD and $r = 0.88$–0.96 for integral vBMD). The weak correlation between aBMD and mechanical properties may be due to several factors, including overestimating aBMD by central DXA due to anatomical features such as irregular geometry, increased bone marrow fat, non-homogeneous fat distribution and the inclusion of posterior spinous processes [11,43,44]. Moreover, DXA cannot provide information on 3D shape, large regional variation in vertebral geometries and the distribution of BMD throughout the bone. Previous studies have also shown that the use of vBMD as a predictor for failure load and failure strength at L3 is stronger than aBMD [45]. Additionally, DXA measured aBMD at L3 or L2-L4 for predicting mechanical properties of the thoracic vertebrae have been evaluated in a previous study, reporting a weaker correlation for the prediction of T10 ($r = 0.62$) compared to L3 ($r = 0.73$) [46]. aBMD measured in the lumbar spine is not intended to predict mechanical properties, particularly at different levels of the spine such as T12 due to the differing mechanical and densitometric properties of the vertebra [46]. This was further confirmed in our study, which demonstrated that changes in mechanical properties at T12 are not reflected by the changes in spine aBMD (L1–L4).

The highest correlation between densitometric and predicted mechanical properties was observed when using integral vBMD. This can be explained considering that the integral vBMD is calculated across the whole vertebral body and provides information from trabecular and cortical bone compartments, both of which contribute to the vertebral

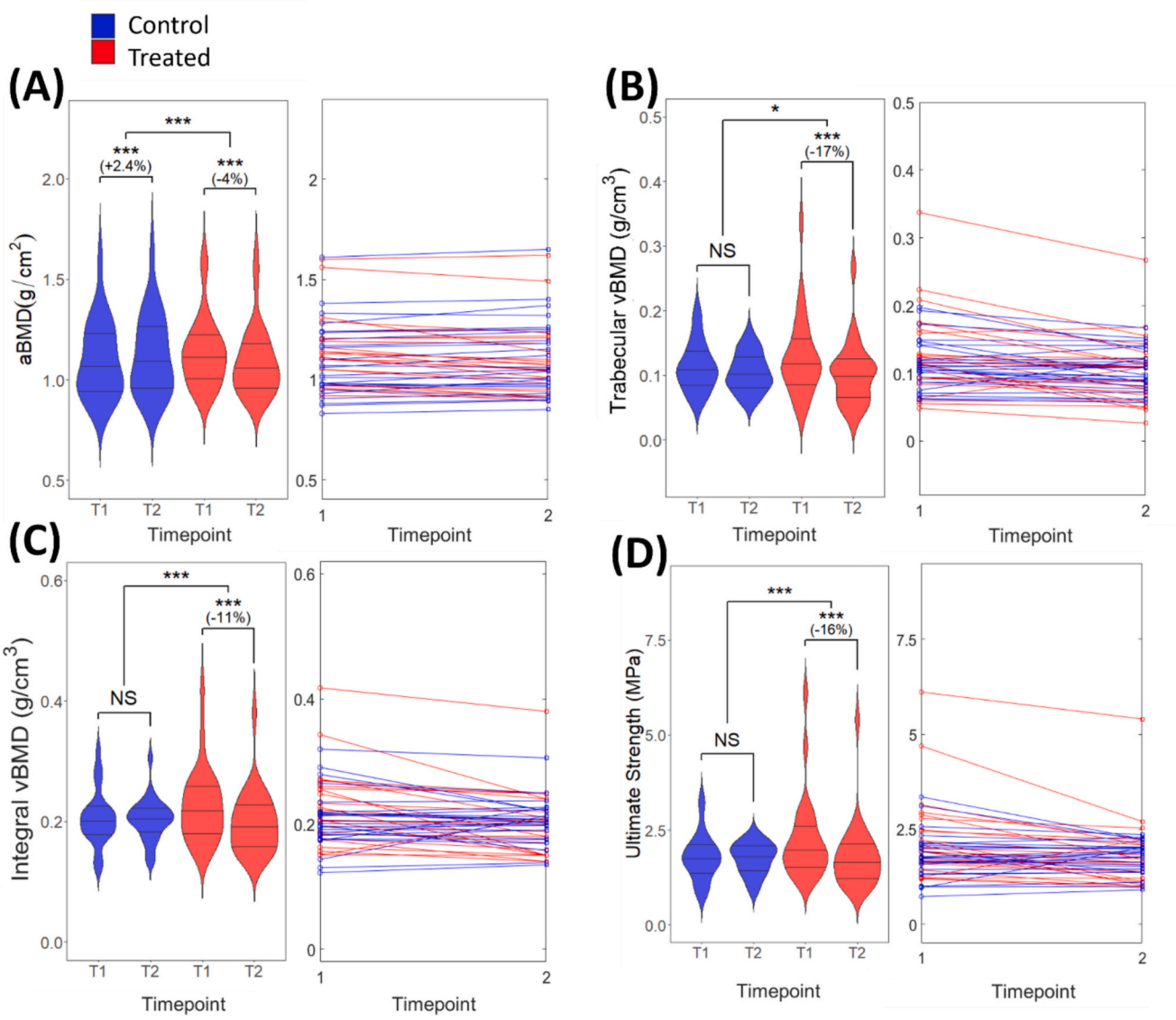

Fig. 5. vBMD and failure strength decrease more than aBMD over 12 months in the treated group. Violin plots of both cohorts and both time points and line plots showing the individual patients within each group for (A) aBMD, (B) trabecular vBMD, (C) integral vBMD, and (D) failure strength. *$p < 0.05$, **$p < 0.01$, ***$p < 0.001$.
Abbreviations: aBMD – areal BMD, vBMD – volumetric BMD, T1 – baseline, T2–12 months.

body compressive strength [47]. The technique adopted here to calculate integral vBMD is not used in the clinical setting. Lower resolution images are acquired clinically and trabecular vBMD is assessed using software available from Mindways (Mindways Software Inc., Austin, TX, USA). However by using integral vBMD, we have demonstrated its improved predictive ability for bone strength compared to aBMD [40,48,49]. Having shown the feasibility of using FE to predict the mechanical strength of vertebrae, this could underpin further work to explore whether improvements in fracture prediction are possible.

Our study has some limitations. Firstly, the material properties of bone were modelled as isotropic. Understanding of the degree of anisotropy can improve the predictive capability of FE models regarding fracture risk in human vertebrae [50]. The inclusion of anisotropy within a FE study has been known to improve the prediction of bone strength in osteoporotic vertebrae [47] and therefore could also improve the biomechanical assessment of PCa patients without the need for higher-dose scans. Nonetheless, the intrinsic anisotropy of the trabecular bone due to the heterogeneous density distribution was captured by using relatively small element size (below 1 mm) and the assignment of heterogeneous material properties in function of the local BMD. It is important to note that any mechanical asymmetry or material anisotropy could affect predictions in complex load cases, but as the vertebrae were loaded in uniaxial compression and the compressive strain was higher than the tensile strain these assumptions are robust for the conditions being modelled. Incorporating other loading conditions such as torsion and bending could improve the assessment of the effect of the ADT on the mechanics of the vertebral body. However, it is well known that compression is the most significant loading condition for most fracture modes and therefore is most used within the field of FE vertebral mechanics [25,48,51]. Another limitation is introduced through the small cohort size within this study. This particularly plays a role in the linear regression analysis towards the larger percentage change in integral and trabecular vBMD where data is sparse. This could be influencing the overall trend and therefore results would need to be confirmed using a larger dataset.

In summary, this study is the first apply finite element modelling to prostate cancer-affected vertebrae, and has shown that ADT treatment for 12 months in a cohort of PCa patients reduces both the densitometric

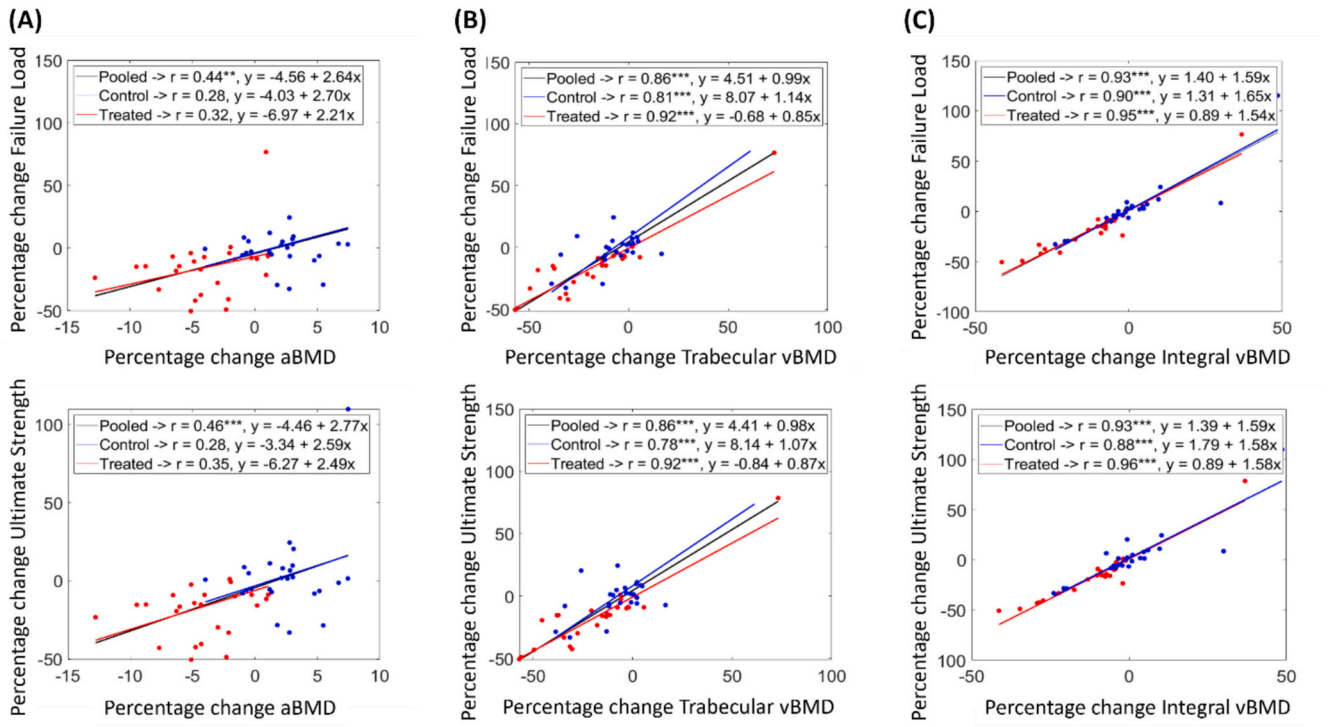

Fig. 6. vBMD has a stronger correlation than aBMD with failure load and failure strength. Linear regression analysis for percentage change failure load and percentage change failure strength vs (A) percentage change aBMD, (B) percentage change trabecular vBMD and (C) percentage change integral vBMD. **p < 0.01, ***p < 0.001.
Abbreviations: aBMD – areal BMD, vBMD – volumetric BMD

and mechanical properties of vertebrae. Despite a similar trend, an amplified reduction was seen for trabecular vBMD, integral vBMD and bone strength compared to aBMD. In addition, the regression analysis confirmed a stronger correlation of both trabecular vBMD and integral vBMD with the mechanical properties than the aBMD, suggesting that the determination of the vBMD might be of higher value when assessing patients bone strength at specific vertebral levels in clinical practice.

CRediT authorship contribution statement

Fiona G. Gibson: Writing – review & editing, Writing – original draft, Visualization, Validation, Methodology, Investigation, Formal analysis, Data curation. **Margaret A. Paggiosi:** Writing – review & editing, Validation, Supervision, Resources, Project administration, Methodology, Investigation, Formal analysis, Data curation. **Catherine Handforth:** Visualization, Validation, Methodology, Investigation, Formal analysis, Data curation. **Janet E. Brown:** Writing – review & editing, Writing – original draft, Visualization, Validation, Supervision, Resources, Project administration, Methodology, Investigation, Funding acquisition, Data curation, Conceptualization. **Xinshan Li:** Writing – review & editing, Visualization, Validation, Supervision, Resources, Project administration, Methodology. **Enrico Dall'Ara:** Writing – review & editing, Visualization, Validation, Supervision, Resources, Project administration, Methodology, Conceptualization. **Stefaan W. Verbruggen:** Writing – review & editing, Writing – original draft, Visualization, Validation, Supervision, Resources, Project administration, Methodology, Investigation, Funding acquisition, Conceptualization.

Funding sources

This work was partially supported by the Weston Park Cancer Charity, Sheffield [Grant number: CA133], by the Engineering and Physical Sciences Research Council (EPSRC) Frontier Multisim Grant (EP/K03877X/1 and EP/S032940/1) and by EPSRC grant (EP/Y001842/1) (SWV). This work forms part of the research portfolio of the National Institute for Health Research Barts Biomedical Research Centre (#NIHR203330).

Declaration of competing interest

The authors declare that they have no known competing financial interests or personal relationships that could have appeared to influence the work reported in this paper.

Acknowledgements

We would like to thank all the ANTELOPE trial participants.

Data availability

The data that support the findings of this study are available on reasonable request from the corresponding author. All requests will be reviewed by relevant stakeholders on the basis of a controlled access approach. The data are not publicly available due to ethical restrictions.

References

[1] A. Jemal, R. Siegel, J. Xu, E. Ward, Cancer statistics, 2010, CA, Cancer J. Clin. 60 (2010) 277–300, https://doi.org/10.3322/CAAC.20073.
[2] P. Rawla, Epidemiology of prostate cancer, World. J. Oncol. 10 (2019) 63, https://doi.org/10.14740/WJON1191.
[3] P.J. Saylor, R.A. Morton, M.L. Hancock, K. Gary Barnette, M.S. Steiner, M.R. Smith, Factors associated with vertebral fractures in men treated with androgen deprivation therapy for prostate cancer abbreviations and acronyms ADT androgen deprivation therapy BMD bone mineral density BMI body mass index BSAP bone specific alkaline phosphatase CTX C-telopeptide GnRH gonadotropin-releasing hormone, J. Urol. 186 (2011) 482–486, https://doi.org/10.1016/j.juro.2011.03.111.
[4] G. Anderson, J. O'Sullivan, Increased fracture risk in prostate cancer: causes and consequences, Trends Urol. Men's Heal. 13 (2022) 6–10, https://doi.org/10.1002/tre.853.

[5] N.D. Shore, Management Review Current and Future Management of Locally Advanced and Metastatic Prostate Cancer KEY WORDS Prostate cancer • Metastatic Prostate cancer • Locally Advanced Prostate Cancer • Androgen Deprivation Therapy • Chemotherapy, 2020.

[6] A.U. Kishan, Y. Sun, H. Hartman, T.M. Pisansky, M. Bolla, A. Neven, A. Steigler, J. W. Denham, F.Y. Feng, A. Zapatero, J.G. Armstrong, A. Nabid, N. Carrier, L. Souhami, M.T. Dunne, J.A. Efstathiou, H.M. Sandler, A. Guerrero, D. Joseph, P. Maingon, T.M. de Reijke, X. Maldonado, T.M. Ma, T. Romero, X. Wang, M. B. Rettig, R.E. Reiter, N.G. Zaorsky, M.L. Steinberg, N.G. Nickols, A.Y. Jia, J. A. Garcia, D.E. Spratt, Androgen deprivation therapy use and duration with definitive radiotherapy for localised prostate cancer: an individual patient data meta-analysis, Lancet Oncol. 23 (2022) 304–316, https://doi.org/10.1016/S1470-2045(21)00705-1.

[7] B. Abrahamsen, M.F. Nielsen, P. Eskildsen, J.T. Andersen, S. Walter, K. Brixen, Fracture risk in Danish men with prostate cancer: a nationwide register study, BJU Int. 100 (2007) 749–754, https://doi.org/10.1111/j.1464-410X.2007.07163.x.

[8] V.B. Shahinian, Y.-F. Kuo, J.L. Freeman, J.S. Goodwin, From the departments of general internal medicine, N. Engl. J. Med. 352 (2005) 154–164. www.nejm.org.

[9] M.E. Suarez-Almazor, X. Pundole, G. Cabanillas, X. Lei, H. Zhao, L.S. Elting, M. A. Lopez-Olivo, S.H. Giordano, Association of bone mineral density testing with risk of major osteoporotic fractures among older men receiving androgen deprivation therapy to treat localized or regional prostate cancer, JAMA Netw. Open 5 (2022) 1–16, https://doi.org/10.1001/jamanetworkopen.2022.5432.

[10] J.E. Brown, C. Handforth, J.E. Compston, W. Cross, N. Parr, P. Selby, S. Wood, L. Drudge-Coates, J.S. Walsh, C. Mitchell, F.J. Collinson, R.E. Coleman, N. James, R. Francis, D.M. Reid, E. McCloskey, Guidance for the assessment and management of prostate cancer treatment-induced bone loss. A consensus position statement from an expert group, J. Bone Oncol. 25 (2020) 100311, https://doi.org/10.1016/j.jbo.2020.100311.

[11] M. Almeida, M.R. Laurent, V. Dubois, F. Claessens, C.A.O. Brien, R. Bouillon, D. Vanderschueren, X.S.C. Manolagas, M. Almeida, V. Dubois, F. Claessens, O. B. Ca, R. Bouillon, Estrogens and Androgens in Skeletal Physiology and Pathophysiology, 2023, pp. 135–187, https://doi.org/10.1152/physrev.00033.2015.

[12] S. Khosla, L. Joseph Melton, B. Lawrence Riggs, Clinical review 144: estrogen and the male skeleton, J. Clin. Endocrinol. Metab. 87 (2002) 1443–1450, https://doi.org/10.1210/jc.87.4.1443.

[13] S.L. Greenspan, P. Coates, S.M. Sereika, J.B. Nelson, D.L. Trump, N.M. Resnick, Bone loss after initiation of androgen deprivation therapy in patients with prostate cancer, J. Clin. Endocrinol. Metab. 90 (2005) 6410–6417, https://doi.org/10.1210/jc.2005-0183.

[14] C.S. Higano, Androgen-deprivation-therapy-induced fractures in men with nonmetastatic prostate cancer: what do we really know? Nat. Clin. Pract. Urol. 5 (2008) 24–34, https://doi.org/10.1038/NCPURO0995.

[15] V. Seifert-Klauss, S. Fillenberg, H. Schneider, P. Luppa, D. Mueller, M. Kiechle, Bone Loss in Premenopausal, Perimenopausal and Postmenopausal Women: Results of a Prospective Observational Study Over 9 Years, Doi:https://doi.org/10.3109/13697137.2012.658110 15 (2012) 433–440. doi:https://doi.org/10.3109/13697137.2012.658110.

[16] M.R. Smith, S.P. Boyce, E. Moyneur, M.S. Duh, M.K. Raut, J. Brandman, Risk of clinical fractures after gonadotropin-releasing hormone agonist therapy for prostate cancer, J. Urol. 175 (2006) 136–139, https://doi.org/10.1016/S0022-5347(05)00033-9.

[17] M.R. Smith, W.C. Lee, J. Brandman, Q. Wang, M. Botteman, C.L. Pashos, Gonadotropin-releasing hormone agonists and fracture risk: a claims-based cohort study of men with nonmetastatic prostate cancer, J. Clin. Oncol. 23 (2005) 7897–7903, https://doi.org/10.1200/JCO.2004.00.6908.

[18] K. Engelke, J.E. Adams, G. Armbrecht, P. Augat, C.E. Bogado, M.L. Bouxsein, D. Felsenberg, M. Ito, S. Prevrhal, D.B. Hans, E.M. Lewiecki, Clinical use of quantitative computed tomography and peripheral quantitative computed tomography in the management of osteoporosis in adults: the 2007 ISCD official positions, J. Clin. Densitom. 11 (2008) 123–162, https://doi.org/10.1016/J.JOCD.2007.12.010.

[19] C. Handforth, M.A. Paggiosi, R. Jacques, F. Gossiel, R. Eastell, J.S. Walsh, J. E. Brown, The impact of androgen deprivation therapy on bone microarchitecture in men with prostate cancer: a longitudinal observational study (the ANTELOPE study), J. Bone Oncol. 47 (2024) 100611, https://doi.org/10.1016/j.jbo.2024.100611.

[20] K. Engelke, B. van Rietbergen, P. Zysset, FEA to measure bone strength: a review, Clin. Rev. Bone Miner. Metab. 14 (2016) 26–37, https://doi.org/10.1007/s12018-015-9201-1.

[21] E. Schileo, F. Taddei, Finite element assessment of bone fragility from clinical images, Curr. Osteoporos. Rep. 19 (2021) 688–698, https://doi.org/10.1007/s11914-021-00714-7.

[22] T. Matsumoto, I. Ohnishi, M. Bessho, K. Imai, S. Ohashi, K. Nakamura, Prediction of vertebral strength under loading conditions occurring in activities of daily living using a computed tomography-based nonlinear finite element method, Spine (Phila Pa 1976) 34 (2009) 1464–1469, https://doi.org/10.1097/BRS.0b013e3181a55636.

[23] M.C. Costa, P. Eltes, A. Lazary, P.P. Varga, M. Viceconti, E. Dall'Ara, Biomechanical assessment of vertebrae with lytic metastases with subject-specific finite element models, J. Mech. Behav. Biomed. Mater. 98 (2019) 268–290, https://doi.org/10.1016/j.jmbbm.2019.06.027.

[24] E. Dall'Ara, D. Pahr, P. Varga, F. Kainberger, P. Zysset, QCT-based finite element models predict human vertebral strength in vitro significantly better than simulated DEXA, Osteoporos. Int. 23 (2012) 563–572, https://doi.org/10.1007/s00198-011-1568-3.

[25] R.P. Crawford, C.E. Cann, T.M. Keaveny, Finite element models predict in vitro vertebral body compressive strength better than quantitative computed tomography, Bone 33 (2003) 744–750, https://doi.org/10.1016/S8756-3282(03)00210-2.

[26] K. Imai, Computed tomography-based finite element analysis to assess fracture risk and osteoporosis treatment, World J. Exp. Med. 5 (2015) 182, https://doi.org/10.5493/wjem.v5.i3.182.

[27] J. Dalla Via, R.M. Daly, P.J. Owen, N.L. Mundell, T. Rantalainen, S.F. Fraser, Bone mineral density, structure, distribution and strength in men with prostate cancer treated with androgen deprivation therapy, Bone 127 (2019) 367–375, https://doi.org/10.1016/j.bone.2019.06.005.

[28] J.K. Lin, C.M. Hearn, E. Getzen, Q. Long, D.C. Lee, T.M. Keaveny, R. Jayadevappa, K.W. Robinson, Y.-N. Wong, K.N. Maxwell, V. Narayan, N.B. Haas, S.U. Takvorian, D.D. Bikle, J.M. Chiang, A.N. Khan, C.S. Rajapakse, A.K. Morgans, R.B. Parikh, Validation of biomechanical computed tomography for fracture risk classification in metastatic hormone-sensitive prostate cancer, Eur. Urol. Oncol. (2023) 1–10, https://doi.org/10.1016/j.euo.2023.10.016.

[29] C.A. Schneider, W.S. Rasband, K.W. Eliceiri, NIH image to ImageJ: 25 years of image analysis, Nat. Methods 9 (2012) 671–675, https://doi.org/10.1038/nmeth.2089.

[30] W. Rasband, ImageJ, U. S. Natl. Institutes Heal., 1997. https://imagej.nih.gov/ij/.

[31] A. Fedorov, R. Beichel, J. Kalpathy-Cramer, J. Finet, J.C. Fillion-Robin, S. Pujol, C. Bauer, D. Jennings, F. Fennessy, M. Sonka, J. Buatti, S. Aylward, J.V. Miller, S. Pieper, R. Kikinis, 3D slicer as an image computing platform for the quantitative imaging network, Magn. Reson. Imaging 30 (2012) 1323, https://doi.org/10.1016/J.MRI.2012.05.001.

[32] E. Schileo, E. Dall'Ara, F. Taddei, A. Malandrino, T. Schotkamp, M. Baleani, M. Viceconti, An accurate estimation of bone density improves the accuracy of subject-specific finite element models, J. Biomech. 41 (2008) 2483–2491, https://doi.org/10.1016/J.JBIOMECH.2008.05.017.

[33] E.F. Morgan, H.H. Bayraktar, T.M. Keaveny, Trabecular bone modulus–density relationships depend on anatomic site, J. Biomech. 36 (2003) 897–904, https://doi.org/10.1016/S0021-9290(03)00071-X.

[34] E.F. Morgan, T.M. Keaveny, Dependence of yield strain of human trabecular bone on anatomic site, J. Biomech. 34 (2001) 569–577, https://doi.org/10.1016/S0021-9290(01)00011-2.

[35] G.L. Niebur, M.J. Feldstein, J.C. Yuen, T.J. Chen, T.M. Keaveny, High-resolution finite element models with tissue strength asymmetry accurately predict failure of trabecular bone, J. Biomech. 33 (2000) 1575–1583, https://doi.org/10.1016/S0021-9290(00)00149-4.

[36] T.M. Keaveny, M.R. McClung, H.K. Genant, J.R. Zanchetta, D. Kendler, J.P. Brown, S. Goemaere, C. Recknor, M.L. Brandi, R. Eastell, D.L. Kopperdahl, K. Engelke, T. Fuerst, H.S. Radcliffe, C. Libanati, Femoral and vertebral strength improvements in postmenopausal women with osteoporosis treated with denosumab, J. Bone Miner. Res. 29 (2014) 158–165, https://doi.org/10.1002/JBMR.2024.

[37] M. Sato, M. Kashii, T. Maekawa, S. Mori, S. Umeda, Y. Kujime, M. Matsushita, S. Kamido, N. Ueda, J. Nakayama, N. Tei, O. Miyake, Impact of androgen deprivation therapy on lumbar spine bone health using quantitative computed tomography in a propensity-matched cohort of patients with prostate cancer, JU Open Plus 2 (2024), https://doi.org/10.1097/ju9.0000000000000158.

[38] M.R. Smith, F.J. McGovern, A.L. Zietman, M.A. Fallon, D.L. Hayden, D. A. Schoenfeld, P.W. Kantoff, J.S. Finkelstein, Pamidronate to prevent bone loss during androgen-deprivation therapy for prostate cancer background treatment with a gonadotropin-releas, N. Engl. J. Med. 948 (2001). www.nejm.org.

[39] K. Imai, I. Ohnishi, S. Yamamoto, K. Nakamura, In vivo assessment of lumbar vertebral strength in elderly women using computed tomography-based nonlinear finite element model, Spine (Phila Pa 1976) 33 (2008) 27–32, https://doi.org/10.1097/BRS.0B013E31815E3993.

[40] T.M. Keaveny, D.W. Donley, P.F. Hoffmann, B.H. Mitlak, E.V. Glass, J.A. San Martin, Effects of teriparatide and alendronate on vertebral strength as assessed by finite element modeling of QCT scans in women with osteoporosis, J. Bone Miner. Res. 22 (2007) 149–157, https://doi.org/10.1359/JBMR.061011.

[41] L.J. Melton, B.L. Riggs, T.M. Keaveny, S.J. Achenbach, D. Kopperdahl, J.J. Camp, P.A. Rouleau, S. Amin, E.J. Atkinson, R.A. Robb, T.M. Therneau, S. Khosla, Relation of vertebral deformities to bone density, structure, and strength, J. Bone Miner. Res. 25 (2010) 1922–1930, https://doi.org/10.1002/JBMR.150.

[42] M.A. Stadelmann, D.E. Schenk, G. Maquer, C. Lenherr, F.M. Buck, D.D. Bosshardt, S. Hoppe, N. Theumann, R.N. Alkalay, P.K. Zysset, Conventional finite element models estimate the strength of metastatic human vertebrae despite alterations of the bone's tissue and structure, Bone 141 (2020) 115598, https://doi.org/10.1016/j.bone.2020.115598.

[43] J.L. Grashuis, H.H. Bolotin, H. Sieva, Patient-specific DXA Bone Mineral Density Inaccuracies: Quantitative Effects of Nonuniform Extraosseous Fat Distributions 18, 2003, pp. 1020–1027.

[44] G.M. Blake, J.F. Grif, D.K.W. Yeung, P.C. Leung, I. Fogelman, Effect of Increasing Vertebral Marrow Fat Content on BMD Measurement, T -Score Status and Fracture Risk Prediction by DXA 44, 2009, pp. 495–501, https://doi.org/10.1016/j.bone.2008.11.003.

[45] G. Tatoń, E. Rokita, A. Wróbel, M. Korkosz, Combining areal DXA bone mineral density and vertebrae postero-anterior width improves the prediction of vertebral strength, Skeletal Radiol. 42 (2013) 1717–1725, https://doi.org/10.1007/s00256-013-1723-3.

[46] D.B. Burklein, E. Lochmuller, V. Kuhn, J. Grimm, R. Barkmann, R.M. Uller, F. Eckstein, Correlation of thoracic and lumbar vertebral failure loads with in situ vs. ex situ dual energy X-ray absorptiometry, J. Biomech. 35 (2001) 579–587.
[47] A.J. Fields, S.K. Eswaran, M.G. Jekir, T.M. Keaveny, Role of trabecular microarchitecture in whole-vertebral body biomechanical behavior, J. Bone Miner. Res. 24 (2009) 1523–1530, https://doi.org/10.1359/jbmr.090317.
[48] X. Wang, A. Sanyal, P.M. Cawthon, L. Palermo, M. Jekir, J. Christensen, K. E. Ensrud, S.R. Cummings, E. Orwoll, D.M. Black, T.M. Keaveny, Prediction of new clinical vertebral fractures in elderly men using finite element analysis of CT scans, J. Bone Miner. Res. 27 (2012) 808–816, https://doi.org/10.1002/JBMR.1539.
[49] L.J. Melton, B.L. Riggs, T.M. Keaveny, S.J. Achenbach, P.F. Hoffmann, J.J. Camp, P.A. Rouleau, M.L. Bouxsein, S. Amin, E.J. Atkinson, R.A. Robb, S. Khosla, Structural determinants of vertebral fracture risk, J. Bone Miner. Res. 22 (2007) 1885–1892, https://doi.org/10.1359/jbmr.070728.
[50] J. Vivanco, P.A. Anderson, E.L. Smith, Dependence of Anisotropy of Human Lumbar Vertebral Trabecular Bone on Quantitative Computed Tomography-based Apparent Density 136, 2014, pp. 1–10, https://doi.org/10.1115/1.4027663.
[51] J.M. Buckley, K. Loo, J. Motherway, Comparison of quantitative computed tomography-based measures in predicting vertebral compressive strength, Bone 40 (2007) 767–774, https://doi.org/10.1016/j.bone.2006.10.025.
[52] Eimear B. Dolan, Stefaan W. Verbruggen, Rebecca A. Rolfe, Chapter 1 - Techniques for studying mechanobiology, in: Stefaan W. Verbruggen (Ed.), Mechanobiology in Health and Disease, Academic Press, 2018, ISBN 9780128129524, pp. 1–53, https://doi.org/10.1016/B978-0-12-812952-4.00001-5.